Experimental Hematology

Experimental Hematology 2016;44:745–754

Biological implications of somatic DDX41 p.R525H mutation in acute myeloid leukemia

Moe Kadono[a,b], Akinori Kanai[a], Akiko Nagamachi[a], Satoru Shinriki[c,d], Jin Kawata[d], Koji Iwato[e], Taiichi Kyo[e], Kumi Oshima[b], Akihiko Yokoyama[f], Takeshi Kawamura[g], Reina Nagase[h], Daichi Inoue[h], Toshio Kitamura[h], Toshiya Inaba[a], Tatsuo Ichinohe[b], and Hirotaka Matsui[a,c,d]

[a]*Department of Molecular Oncology and Leukemia Program Project, Research Institute for Radiation Biology and Medicine, Hiroshima University, Hiroshima, Japan;* [b]*Department of Hematology and Oncology, Research Institute for Radiation Biology and Medicine, Hiroshima University, Hiroshima, Japan;* [c]*Department of Molecular Laboratory Medicine, Graduate School of Medical Sciences, Kumamoto University, Kumamoto, Japan;* [d]*Central Clinical Laboratory, Kumamoto University Hospital, Kumamoto, Japan;* [e]*Department of Hematology, Hiroshima Red Cross Hospital & Atomic-bomb Survivors Hospital, Hiroshima, Japan;* [f]*Laboratory for Malignancy Control Research, Medical Innovation Center, Kyoto University Graduate School of Medicine, Kyoto, Japan;* [g]*Department of Molecular Biology and Medicine, Laboratory for System Biology and Medicine (LSBM), Research Center for Advanced Science and Technology (RCAST), University of Tokyo, Tokyo, Japan;* [h]*Division of Cellular Therapy, Institute of Medical Science, The University of Tokyo, Tokyo, Japan*

(Received 13 April 2016; revised 28 April 2016; accepted 29 April 2016)

The *DDX41* gene, encoding a DEAD-box type ATP-dependent RNA helicase, is rarely but reproducibly mutated in myeloid diseases. The acquired mutation in *DDX41* is highly concentrated at c.G1574A (p.R525H) in the conserved motif VI located at the C-terminus of the helicase core domain where ATP interacts and is hydrolyzed. Therefore, it is likely that the p.R525H mutation perturbs ATPase activity in a dominant-negative manner. In this study, we screened for the *DDX41* mutation of CD34-positive tumor cells based on mRNA sequencing and identified the p.R525H mutation in three cases among 23 patients. Intriguingly, these patients commonly exhibited acute myeloid leukemia (AML) with peripheral blood cytopenias and low blast counts, suggesting that the mutation inhibits the growth and differentiation of hematopoietic cells. Data from cord blood cells and leukemia cell lines suggest a role for DDX41 in preribosomal RNA processing, in which the expression of the p.R525H mutant causes a certain ribosomopathy phenotype in hematopoietic cells by suppressing MDM2-mediated RB degradation, thus triggering the inhibition of E2F activity. This study uncovered a pathogenic role of p.R525H DDX41 in the slow growth rate of tumor cells. Age-dependent epigenetic alterations or other somatic changes might collaborate with the mutation to cause AML.

Current comprehensive sequencing approaches led to the identification of rare but reproducible somatic gene mutations in myeloid malignancies. Among them, there is a somatic mutation in the *DDX41* gene encoding a DEAD-box type ATP-dependent RNA helicase. The somatic mutation in *DDX41* is highly concentrated at c.G1574A (p.R525H) in the conserved motif VI, located at the C-terminus of the RecA-like helicase core domain where ATP interacts and is hydrolyzed. Therefore, it is likely that the p.R525H mutation in the DDX41 protein perturbs ATPase activity in a dominant-negative manner. In addition, germline mutations in *DDX41* were recently isolated in a subset of familial acute myeloid leukemia (AML)/myelodysplastic syndrome (MDS) pedigrees [1,2]. Because the roles of these somatic and germline mutations in the pathogenesis of myeloid diseases are not completely understood, the researchers who first described these mutations advocate a role for DDX41 in mRNA splicing via

Offprint requests to: Hirotaka Matsui, Department of Molecular Laboratory Medicine, Graduate School of Medical Sciences, Kumamoto University, 1-1-1 Honjo, Chuo-ku, Kumamoto, Japan 860-8556; E-mail: hmatsui@kumamoto-u.ac.jp or Tatsuo Ichinohe, MD, PhD, Department of Hematology and Oncology, Research Institute for Radiation Biology and Medicine, Hiroshima University, 1-2-3 Kasumi, Minami-ku, Hiroshima, Japan 784-8553; E-mail: nohe@hiroshima-u.ac.jp

Supplementary data related to this article can be found at http://dx.doi.org/10.1016/j.exphem.2016.04.017.

http://dx.doi.org/10.1016/j.exphem.2016.04.017

interaction with the U2 and U5 complexes [1]. However, unlike canonical spliceosomal mutations, the *DDX41* mutation causes, not only MDS, but also primary AML.

In this study, we propose a role for DDX41 as a precursor ribosome RNA (pre-rRNA) processing factor in which the p.R525H mutation affects ribosome biogenesis. We found that ribosome biogenesis was affected widely when cord blood–derived CD34-positive cells were transfected with DDX41 p.R525H, thus compromising cell cycle progression through impaired E2F function. Because molecular mechanisms for the development of AML with cytopenias have not been elucidated, we propose here that the DDX41 p.R525H mutation in hematopoietic stem/progenitor cells is involved in the pathogenesis of a certain subset of such AML cases.

Methods

Patient samples and cell fractionation

Bone marrow aspirates or peripheral blood specimens were collected from 23 patients with AML who participated in the study according to the protocol approved by the ethics committee on human genome research at Hiroshima University and Kumamoto University. The protocol was based on an opt-out or on written informed consent obtained by the patients. The protocol included the use of pooled samples at initial diagnosis. Total RNA was extracted from CD34-positive cell fractions isolated by magnetic activated cell sorting. Where possible, CD3-positive and CD34-negative/CD3-negative fractions were isolated.

mRNA sequencing

In this study, gene mutations were screened upon mRNA sequencing. The libraries for mRNA sequencing were prepared according to the SureSelect library preparation kit (Agilent Technologies, Santa Clara, CA) and subjected to massively parallel sequencing with a GAIIX or Hiseq2500 sequencer (Illumina, San Diego, CA) using a single-end 36-bp or 50-bp sequencing length protocol. Sequenced tags were aligned to the human reference genome (build hg19) using ELAND (Illumina), and gene expression was normalized to the amount of reads per kilobase of exon per million mapped (rpkm).

Antibodies

The following antibodies were used in this study: anti-DDX41 (ab182007; Abcam, Cambridge, UK), anti-Actin (MAB1501; Merck Millipore, Darmstadt, Germany), anti-FLAG M2 (F3165; Sigma-Aldrich, St. Louis, MO), anti-Myc-tag (2272; Cell Signaling Technology, Danvers, MA), anti-Nucleolin (M019-3S; MBL, Nagoya, Japan), anti-RPL5 (ab86863; Abcam), anti-RPL11 (ab79352; Abcam), anti-RB (9313; Cell Signaling Technology), anti-phospho-RB (9301; Cell Signaling Technology), anti-MDM2 (ab3110; Abcam), and anti–multi-ubiquitin (D058-3; MBL).

Vector construction

DDX41 and other cDNAs used in this study were obtained by polymerase chain reaction (PCR) amplification from human cord blood–derived total RNA and cloned into pMYs-IG retrovirus vector [3]. Point mutations and truncations were generated using a site-directed mutagenesis approach.

Cell culture and plasmid transfection

Cord blood–derived CD34-positive cells were purchased from the RIKEN Cell Bank (Ibaraki, Japan). The cells were cultured on Tst4/min feeder cells (kindly provided by Dr. H. Kawamoto at Kyoto University) in Dulbecco's modified Eagle medium supplemented with 20% fetal bovine serum (FBS) in the presence of human stem cell factor (SCF), FMS-related tyrosine kinase 3 ligand (FLT3-L), and thrombopoietin (TPO; 100 ng/mL each). THP-1 and K562 cells were cultured in RPMI1640 medium containing 10% FBS. For enforced gene expression, pMYs-IG retroviral vector and PLAT-E or PLAT-F packaging cells were used.

Immunofluorescence analysis

Murine lung fibroblasts grown on coverslips were infected with a retrovirus and cultured for 2 days. THP-1 cells were first transduced with retrovirus and then attached to a glass slide using a cytospin apparatus. The cells were fixed with 4% paraformaldehyde, permeabilized with 0.1% Triton X-100, and blocked with 1% bovine serum albumin (BSA), followed by staining with primary antibodies. After staining with Cy3-or Alexa Fluor 488-labeled secondary antibodies and Hoechst 33342, fluorescent signals were observed, and the images were taken using a confocal laser scanning microscope (LSM 5; Carl Zeiss Microscopy, Jena, Germany).

Immunoblot and immunoprecipitation analysis

Cells (1×10^6) were extracted with NP40 lysis buffer (50 mM Tris-HCl pH 8.0, 150 mM NaCl, and 1.0% NP40) containing proteinase and phosphatase inhibitor cocktails (Complete and PhosSTOP; Roche Life Sciences, Indianapolis, IN). For immunoprecipitation analysis, protein G-coated magnet beads (20 μL in each experiment) were conjugated with an antibody (4 μg) and mixed with cell extracts overnight at 4°C. The beads were washed five times with NP40 lysis buffer and then resuspended with 50 μL of sample buffer (NP40 lysis buffer containing 1% sodium dodecyl sulfate, 0.5% β-mercaptoethanol, and 12.5% glycerol), followed by denaturation and elution by heating at 95°C for 2 minutes. The samples were loaded and electrophoresed on 8.5%, 12.5%, or 15% polyacrylamide gels according to the molecular weight of the protein of interest.

Northern blotting analysis

Northern blotting analysis was performed based on a non-RI protocol according to the manufacturer's instructions (DIG Northern Starter Kit; Roche Life Sciences). Briefly, 1.5 μg of total RNA was denatured and fractionated using a denaturing gel (2% formaldehyde/1.2% agarose), followed by transfer to a nylon membrane. The membranes were hybridized with digoxigenin-labeled RNA probes, and the signals were detected using alkaline-phosphatase–labeled antidigoxigenin antibody and a chemiluminescent substrate. RNA probes in this assay were prepared by PCR amplification of internal transcribed spacer 1 (ITS1) and ITS2 regions (for ITS1, forward primer: 5′-acggagcccggagggcgaggcccgc-3′, reverse primer: 5′-cgtctccctcccgagttctcggctc-3′; and for ITS2, forward primer: 5′- ctaagcgcagacccggcggcgtccg-3′, reverse primer: 5′- acgggaactcggcccgagccggctc-3′), followed by in vitro transcription using DIG-11-UTP for probe labeling. The ITS1 probe was used for the identification of 47S, 45S, 30S, and 21S pre-rRNA, whereas the ITS2 probe was used for 47S, 45S, 32S, and 12S detection (Supplementary Figures E1A and E1B, online only,

available at www.exphem.org). Schematic pre-rRNA–processing pathways are shown in Supplementary Figure E1B.

ATPase assay

The assay reaction (10 μL) contained the following components: 50 mM Tris-HCl, pH 7.4, 20 mM $MgCl_2$, 50 mM KCl, 3.33 pM [α-^{32}P]ATP, and 0.2 μg of helicase domain of DDX41 purified by an in vitro translation system (Trans-direct insect cell; Shimadzu, Kyoto, Japan). BSA was used as a negative control. Samples were incubated for 15 or 30 minutes at 37°C, and the reaction was stopped by adding 1 μL of 0.5M EDTA, pH 8.0. The reaction mixture (1 μL) was then spotted on a cellulose PEI-F plate (Avantor Performance Materials, Center Valley, PA) and developed by ascending chromatography in 0.75 M LiCl/1 M formic acid solution for 1 hour. The plate was air dried and the ATP/ADP signals were detected by autoradiography.

Mouse bone marrow transplantation (BMT)

C57BL/6 (Ly5.1) mice (Sankyo Labo Service Corporation, Tokyo, Japan) and C57BL/6 (Ly5.2) mice (Charles River Laboratories Japan, Kanagawa, Japan) were used for BMT experiments. A total of 100,000 cells (Ly5.1) transduced with a DDX41/GFP expression vector was transplanted into sublethally irradiated recipient mice (Ly5.2), and peripheral white blood cell (WBC) numbers and green fluorescent protein signals were measured 2–3 months later.

Results

Identification of the DDX41 p.R525H mutation in three AML patients

We screened for the *DDX41* mutation of CD34-positive tumor cells based on mRNA sequencing and identified a

A

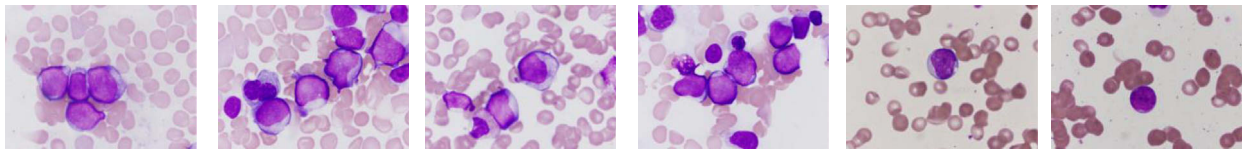

UPN	Age/Sex	Karyotype	WBC (10^3/μL)	Blast(%) (PB)	Blast(%) (BM)	Hb (g/dL)	Plt (10^4/μL)	Other gene mutations*
6	72/M	45,X,-Y (8/20cells), 46,XY (12/20cells)	1.6	1	25	11.3	6.7	*SF1*
10	81/M	47,XY,+der(1;19)(q10;p10) (3/20cells), 46,XY (17/20cells)	0.6	1	32	6.4	1.6	—
17	64/M	46,XY	3.1	3.3	28	4.8	16.6	—
2995 (TCGA)	67/M	46,XY	0.6	0	35	N.I.	N.I.	*MYLK2*

*mutations previously reported as recurrent.
N.I.: not indicated.

B

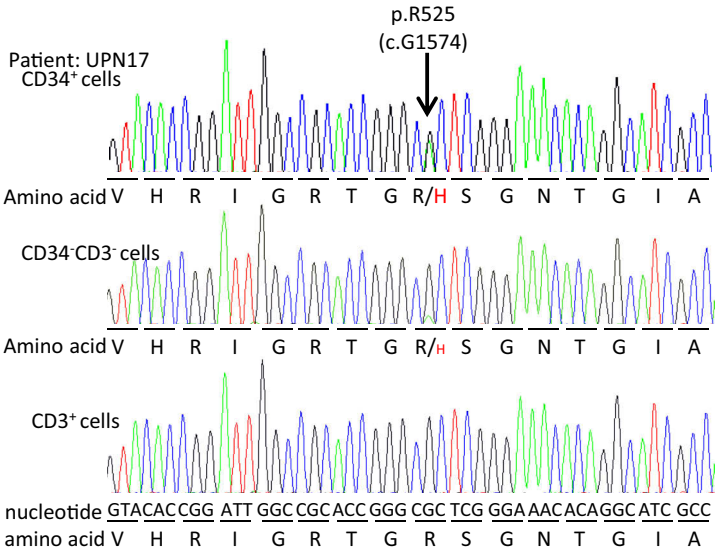

Figure 1. Identification of the somatic DDX41 p.R525H mutation in AML patients exhibiting cytopenias. (**A**) Bone marrow blasts of three AML patients harboring the p.R525H DDX41 mutation. The images were taken at 400× magnification. Clinical manifestations of the patients are shown in the table at the bottom. (**B**) Confirmation of somatic DDX41 p.R525H mutation by Sanger resequencing. Representative data of CD34-positive, CD34-negative/CD3-negative, and CD3-positive cells from patient UPN17 are shown. Arrow indicates the p.R525 position.

heterozygous DDX41 c.G1574A (p.R525H) mutation (chr5: 176,939,370 on build GRCh37/hg19) in three cases among 23 patients (Fig. 1A). Although we did not perform comprehensive sequencing of paired germline DNA, we confirmed the mutation as somatic by the direct genome sequencing of CD3-positive cells (Fig. 1B). Intriguingly, these patients, in addition to a patient with the same mutation enlisted in the Cancer Genome Atlas [4], exhibited AML with peripheral and bone marrow cytopenias and low blast counts (Fig. 1A), although the precise cellularity of the bone marrow was undetermined because a bone marrow biopsy was not performed. In addition, a recent study described a germline p.R525H mutation associated with bone marrow hypocellularity and low WBC count in a primary AML patient [2]. According to our transcriptome data on patients' CD34-positive cells, almost one half of the sequenced tags at c.G1574 were considered mutated in each patient (18 of 37, 19 of 32, and 23 of 47 reads were called "A"). Therefore, almost all CD34-positive cells in these patients may harbor a heterozygous *DDX41* p.R525H mutation, although deeper sequencing analysis is required to assess the precise variant allele frequencies. Conversely, CD34-negative cells carrying the mutation were fewer compared with CD34-positive cells, and CD3-positive cells carrying the mutation were almost absent, as estimated by direct genomic DNA sequencing (Fig. 1B). These data suggest a somatic nature of the mutation in the patient and a block in the differentiation of CD34-positive *DDX41* mutant cells into negative cells.

Nuclear localization of the DDX41 protein

We next clarified the localization of the DDX41 protein. In this experiment, FLAG-tagged STING, a protein that had been reported to interact with DDX41 at the endoplasmic reticulum [5,6], was coexpressed with Myc-tagged DDX41 in fibroblasts. Ectopically expressed DDX41 was mostly nuclear regardless of the p.R525H mutation and minimally colocalized with FLAG-STING in a steady state

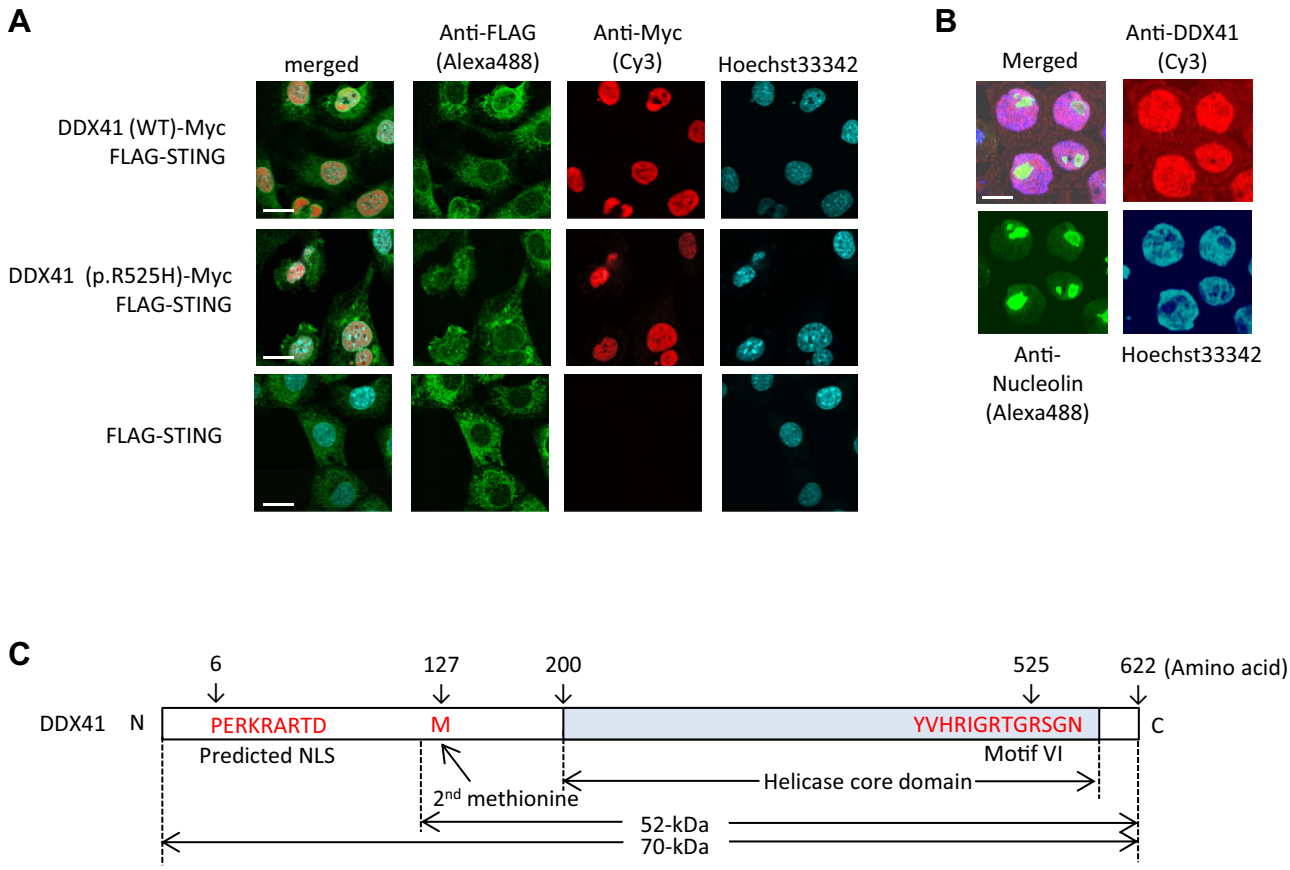

Figure 2. Nuclear localization of DDX41. (**A**) Localization of Myc-tagged human DDX41 protein in murine fibroblasts by immunofluorescent analysis. DDX41 protein with or without a p.R525H substitution was expressed together with a FLAG-tagged STING. An anti-Myc rabbit antibody and an anti-FLAG mouse antibody were used as primary antibodies; a Cy3-labeled antirabbit antibody and Alexa Fluor 488-labeled antimouse antibodies were used as secondary antibodies. Nuclei were stained with Hoechst 33342. Scale bars: 20 μm. (**B**) Endogenous DDX41 expression in THP-1 cells. The cells, attached to a glass slide using a cytospin apparatus, were stained with an anti-DDX41 and an anti-Nucleolin antibody, followed by staining with a Cy3-labeled anti-Rabbit antibody and an Alexa Fluor 488-labeled anti-Mouse antibody, respectively. The images were taken using a LSM-5 PASCAL confocal microscopy. Scale bar, 20 μm. (**C**) Schematic illustration of the DDX41 protein structure. The helicase core domain is shown in *light blue*. A predicted NLS, the second methionine, and the motif VI in the helicase domain are shown in *red*.

(Fig. 2A). In the THP-1 leukemia cell line, the endogenous DDX41 protein was also mostly nuclear (Fig. 2B). In the nucleus, DDX41 protein localized both in the nucleoplasm and in the nucleolus (stained with nucleolin), suggesting that DDX41 plays a role in the nucleoplasm as well as in the nucleolus. Although previous studies described DDX41 as a cytosolic DNA sensor that recognizes nucleic acids of pathogens [6], our study did not suggest this function based on the protein localization. However, we identified a 52-kDa DDX41 short isoform translated from the second methionine in addition to the full-length 70-kDa DDX41 (Fig. 2C; Supplementary Figures E2A and E2B, online only, available at www.exphem.org). This short form, which lacks a putative nuclear localizing signal (NLS) and is detected both in the cytoplasm and in the nucleus (Fig. 2C; Supplementary Figure E2C, online only, available at www.exphem.org), might function as a sensor of pathogenic nucleic acids.

Growth inhibition of p.R525H DDX41-expressing cells due to impaired pre-rRNA processing

To investigate the molecular functions of DDX41 in hematopoietic cells, cord blood–derived human CD34-positive cells were transduced with wild-type (WT) or p.R525H DDX41 using a retroviral system [3], followed by cultivation in the presence of 100 ng/mL SCF, TPO, and FLT3-L. After a 30-day culture, p.R525H cells showed decreased proliferation compared with WT cells (Fig. 3A), and this was accompanied by the suppression of mRNAs encoding ribosomal proteins (Supplementary Figure E3A, online only, available at www.exphem.org). A gene set enrichment analysis (GSEA) [7] showed that the gene expression pattern of p.R525H cells was negatively correlated with ribosomal gene sets and with myc target genes (Supplementary Figure E3B, online only, available at www.exphem.org). GSEA further indicated an enrichment of the genes upregulated in the absence of RPS14 in p.R525H cells (Supplementary Figure E3B). These data suggest that a certain ribosomopathy [8] may occur in the mutant DDX41-expressing cells.

These findings and a highly conserved DEAD-box type RNA helicase domain of DDX41 led us to speculate that the DDX41 protein might be involved in pre-rRNA processing. A recent study also supports this speculation [9]. As expected from the position of the somatic mutation (p.R525), which is within the helicase core where the ATP binds and is hydrolyzed (Fig. 2C) [10], the mutant helicase domain displayed a lower ATPase activity (Fig. 3B). In addition, northern blot analysis probing ITS1 and ITS2 of pre-rRNA showed increased signals of 47S and 41S pre-rRNAs (Fig. 3C). The 30S signal was slightly upregulated, whereas the 21S signal was decreased in THP-1 cells expressing p.R525H DDX41. Instead, the 32S signal was increased both in WT and p.R525H cells. Furthermore, semiquantitative real-time PCR experiments showed relatively higher amounts of pre-rRNA containing 5′ external transcribed spacer (ETS) or ITS2 than that containing ITS1 in p.R525H cord blood cells (Fig. 3D). Although the precise phase at which DDX41 takes part in pre-rRNA processing has not been elucidated, this series of experiments suggests a role for DDX41 in the trimming of 5′ ETS and/or ITS2.

Activation of RB pathway occurring in p.R525H DDX41-expressing cells

As mentioned previously, p.R525H DDX41 cord blood cells were fewer than WT cells after the culture (Fig. 3A), but the induction of apoptosis was unlikely because cell viability was maintained at almost 100% throughout the culture (data not shown). Recent studies on ribosomopathies revealed an activation of the MDM2-p53 pathway in the pathogenesis of the diseases [11,12]. It is now widely recognized that RPL5 and RPL11 not incorporated into the 60S ribosome bind preferentially to

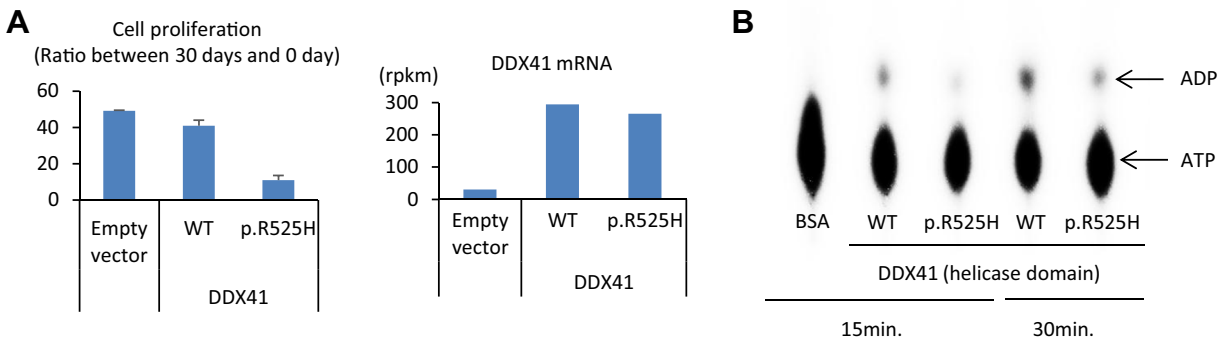

Figure 3. Cell growth inhibition by DDX41 p.R525H mutation that causes impaired ribosomal biogenesis. (**A**) Proliferation of CD34-positive cord blood cells transfected with a DDX41-expressing vector or an empty vector in the presence of SCF, TPO, and FLT3-L. The left graph indicates the ratio between the number of cells at 30 days and at the beginning of the assay. The right graph shows DDX41 mRNA expression levels as indicated by rpkm values. (**B**) ATPase assay using a helicase domain of the DDX41 (WT and p.R525H mutant) protein as catalyst. In vitro-translated helicase domains were mixed with [α-^{32}P]ATP for the indicated minutes, and the mixtures were subjected to thin-layer chromatography. Arrows indicate ATP and ADP.

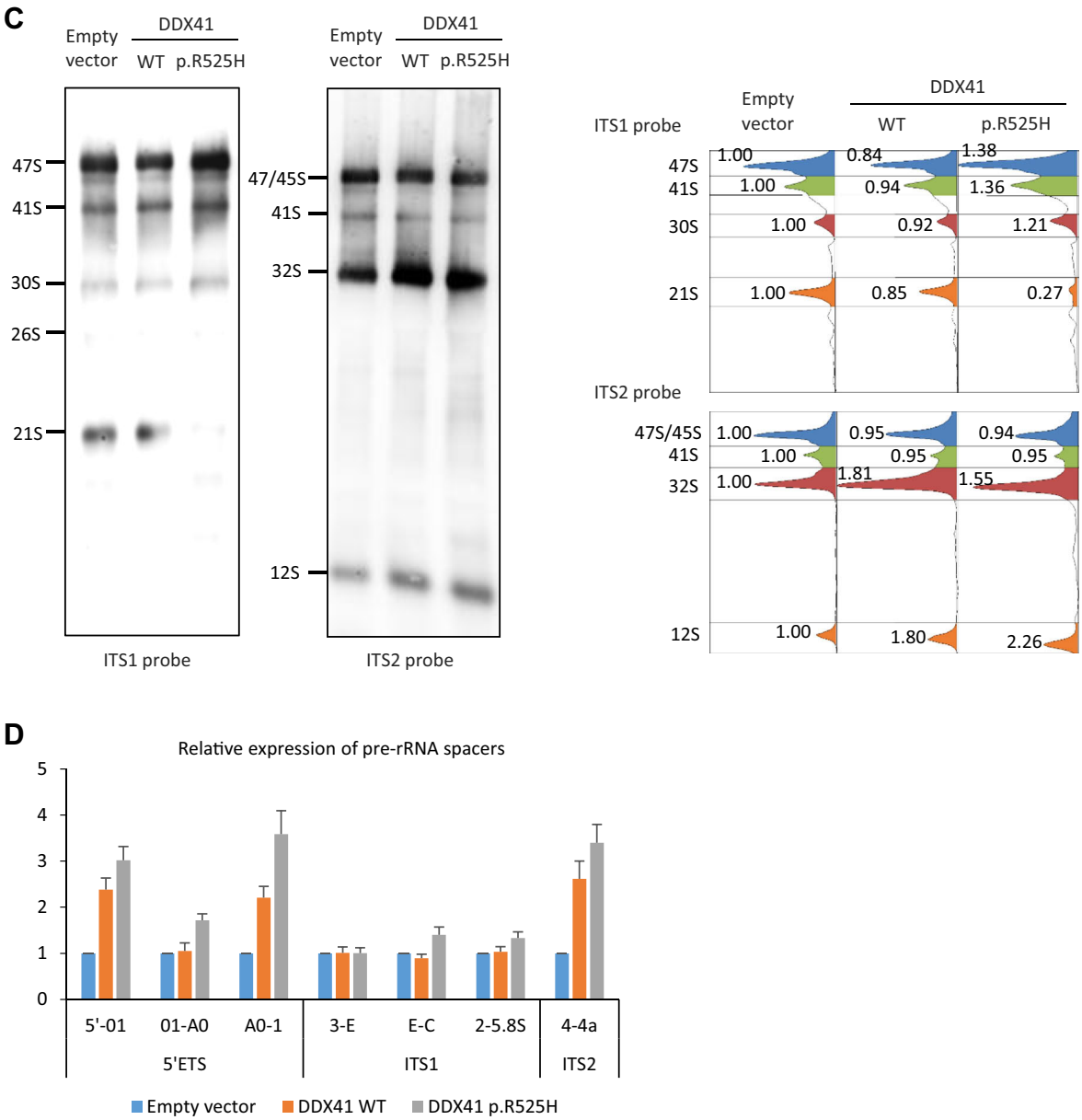

Figure 3. (*continued*) (**C**) Detection of pre-rRNA intermediates expressed in THP-1 cells by northern blotting analysis. DIG-labeled RNA probes for ITS1 and ITS2 regions were used for the detection (Supplementary Figure E1A). The right panels indicate lane profile plots generated from the northern blots (left panels) using ImageJ software and quantitative values of each pre-rRNA band relative to the empty vector control. (**D**) Relative amounts of pre-rRNA spacers as assessed by quantitative PCR analysis. Empty vector or DDX41 (p.R525H and WT)-transfected cord blood cells were subjected to quantitative PCR experiments. The regions amplified by PCR are shown in Supplementary Figure E1A.

MDM2, so inhibition of p53 by MDM2 is compromised, causing a stimulation of the p53 pathway [13,14]. We initially assumed that the same defect might be involved in the growth impairment of p.R525H DDX41 cells. Nevertheless, GSEA did not indicate p53 activation in the cells, probably because we cultured cord blood cells with a combination of cytokines (SCF, FLT3-L, and TPO). This combination is expected to expand hematopoietic stem/progenitor cells with less differentiation. Data from transcriptome analysis suggested no erythroid differentiation in this culture condition, in which globin genes were almost not expressed at all. Given that ribosomal defect-mediated activation of p53 pathway occurs preferentially in the erythroid lineage in ribosomopathies, our culture conditions might not have been optimal to observe p53 activation.

Instead, GSEA revealed a negative enrichment of cell cycle–promoting genes regulated by the RB-E2F axis in p.R525H DDX41 cord blood cells (Fig. 4A). Cell cycle inhibition through the suppression of E2F activity was also detected in patient-derived samples (Fig. 4B). In our study,

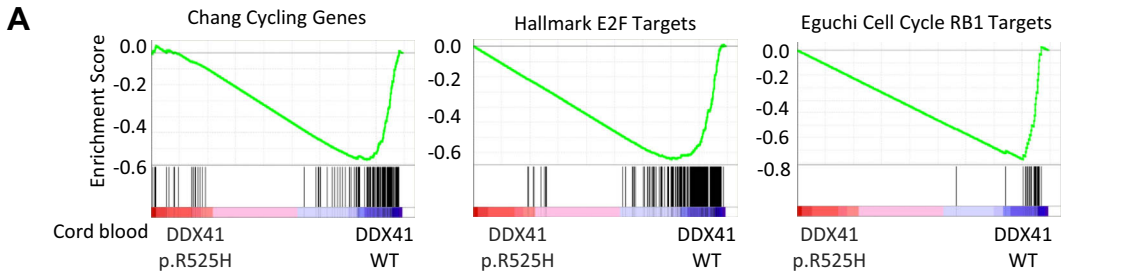

	Chang Cycling Genes	Hallmark E2F Targets	Eguchi Cell Cycle RB1 Targets
Normalized Enrichment Score	-2.14	-2.46	-2.04
Nominal p-value	0.0	0.0	0.0
FDR q-value	0.0	0.0	0.0

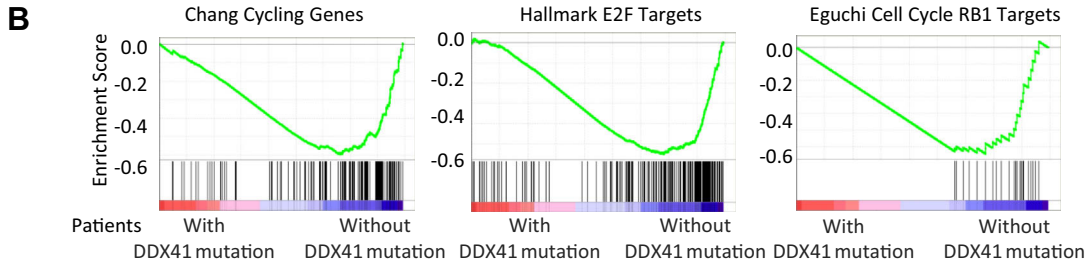

	Chang Cycling Genes	Hallmark E2F Targets	Eguchi Cell Cycle RB1 Targets
Normalized Enrichment Score	-2.30	-2.19	-1.80
Nominal p-value	0.0	0.0	0.0
FDR q-value	0.0	0.0	0.02

Figure 4. Ribosomal stress that results in the activation of RB pathway occurring in p.R525H-expressing cells. (**A**) Negative enrichment of cell cycle–promoting genes regulated by the RB-E2F axis in DDX41 p.R525H cord blood cells. GSEA analyses were performed using mRNA-sequencing data in which the plots of "Chang Cycling Genes," "Hallmark E2F Targets," and "Eguchi Cell Cycle RB1 Targets" are shown as representatives. Normalized enrichment score, nominal p value, and false discovery rate (FDR) q value are indicated at the bottom. (**B**) Negative enrichment of cell cycle–promoting genes regulated by the RB-E2F axis in CD34-positive tumor cells obtained from patients (three patients with the p.R525H mutation were compared with 20 patients without the mutation). GSEA analyses were performed as in (**A**).

we found increased RPL5 and RPL11 bound to MDM2 in p.R525H DDX41 cells (Fig. 4C). Because the total amount of these ribosomal proteins was apparently not altered by the enforced expression of p.R525H DDX41, the mutant DDX41 might increase free ribosomal proteins that are not incorporated into the 60S ribosome, and these proteins may eventually form a complex with MDM2. Moreover, the RB protein was increased in p.R525H DDX41 cells, in part due to the inhibition of MDM2-mediated poly-ubiquitination (Fig. 4D). The RB protein was active in p.R525H DDX41 cells because it was dephosphorylated, although the mechanism of the dephosphorylation is currently unclear. Furthermore, impaired growth was observed in p.R525H DDX41 THP-1 cells lacking WT p53 (Supplementary Figure E4A, online only, available at www.exphem.org) [15], implying a p53-independent but RB-dependent cell cycle inhibition by the mutant DDX41.

Discussion

In this study, we performed mRNA sequencing on 23 patients and identified the DDX41 p.R525H mutation in three AML patients. The rate of somatic DDX41 mutation was high compared with previous studies because of our limited number of patients or because of the use of CD34-positive cells in our study. In most previous studies, whole genome or exome sequencing was performed using total bone marrow or peripheral blood specimens. Given that tumor cells harboring the DDX41 mutation rarely divide and differentiate, a screening using whole hematopoietic cells might fail to detect mutations of such a rare population, thus underestimating the rate of DDX41 mutation among AML/MDS patients.

DDX41 protein is a DEAD-box type ATP-dependent RNA helicase [10] in which the helicase domain is highly conserved. DEAD-box RNA helicases have been shown to act in many pathways, including pre-mRNA splicing and ribosome biogenesis. In addition, recent studies propose roles of RNA helicases, such as RIG-I, in sensing nucleic acids of microbes incorporated into cells [16,17]. In addition, some DEAD-box RNA helicases have multiple functions and have been involved in tumorigenesis [18,19]. However, the function of DDX41 has not been investigated until recently. A recent study reported that DDX41 cooperates with mRNA-splicing

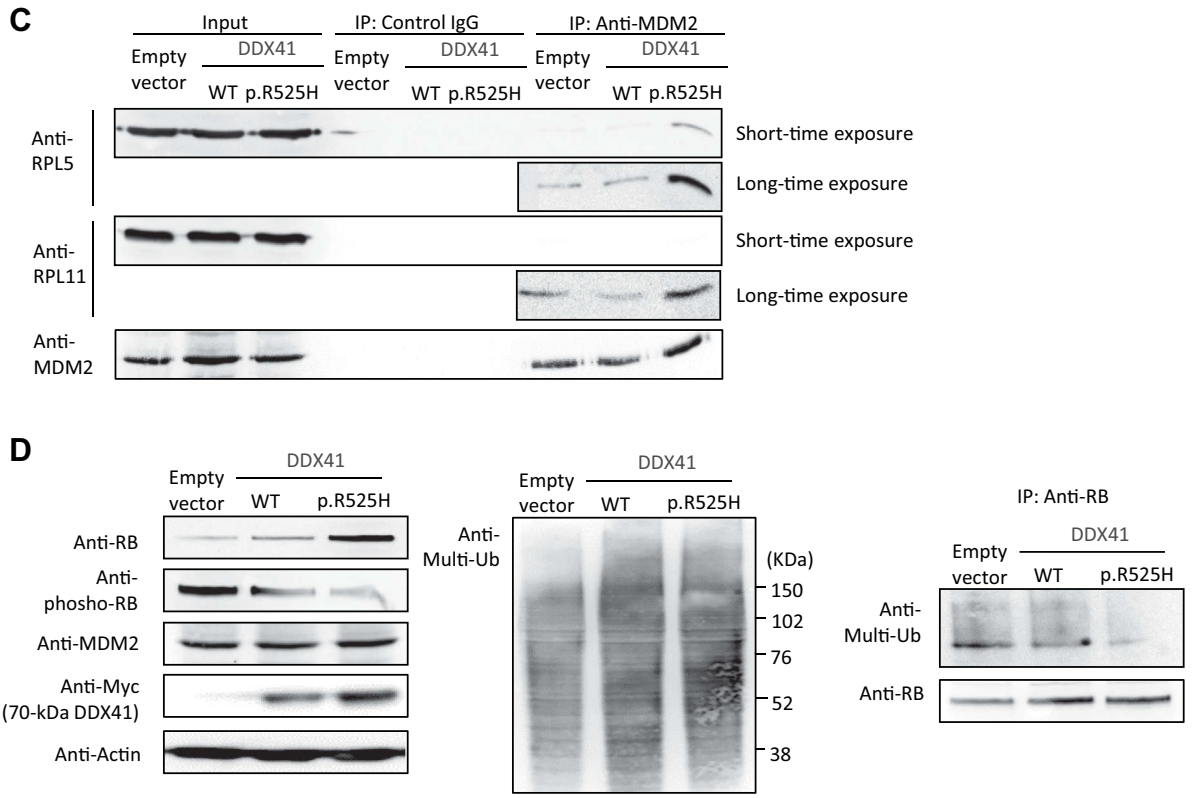

Figure 4. (*continued*) (**C**) Increased binding of RPL5 and RPL11 to MDM2 in p.R525H DDX41-expressing cells. Total protein extracts from K562 cells expressing DDX41 (WT or p.R525H) or those transfected with an empty vector were subjected to immunoprecipitation analysis using an anti-MDM2 antibody or a control IgG, followed by the detection of the RPL5, RPL11, and MDM2 proteins. (**D**) Expression of RB and its phosphorylated and polyubiquitinated forms of MDM2, Myc-tagged DDX41, actin, and polyubiquitinated proteins in K562 cells transfected with an empty vector or with a DDX41 (WT or p.R525H) vector. In the immunoprecipitation analysis (right panels indicated as IP), proteins precipitated with an anti-RB antibody were blotted using an anti–multi-ubiquitin antibody and an anti-RB antibody.

factors and is involved in late spliceosomal processing [1]. However, as we mentioned previously, we identified a DDX41 p.R525H mutation in AML patients exhibiting cytopenias in bone marrow and peripheral blood, the pathogenesis of which has not been known to be connected to mRNA splicing defect. Therefore, we further investigated the biological functions of DDX41 and its contribution to the development of AML through an acquired mutation.

The DDX41 localizes at the nuclear matrix and in the nucleolus, consistent with the putative NLS at the N-terminus. However, contrary to our observation, a recent study described DDX41 localization in the cytoplasm even when a full-length cDNA was transfected [6]. The reason for the discrepancy between our observation and observations from others is not obvious, but it might be possible that a short form that we identified for the first time in this study was mainly expressed in previous studies describing DDX41 in the cytoplasm. Because it has also been reported that human DDX41 shuttles between the nucleus and cytoplasm [20], it could be also possible that cells in which DDX41 is localized mainly in the cytoplasm were used in previous studies.

Although the enforced expression of WT DDX41 in cord blood–derived cells had minimal effects, substitution of p.R525 into histidine induced cell cycle arrest, suggesting that this alteration interferes with cell growth in a dominant-negative manner. In addition, as expected, the inhibitory effect of p.R525H DDX41 on cell cycle progression is due to the loss of ATPase activity. Unexpectedly, the cell cycle arrest was MDM2-and RB-dependent, but p53-independent. However, this is consistent with previous studies arguing that MDM2-dependent but p53-independent pathways also cause ribosomopathies [21,22].

Our results further indicate an interference of p.R525H DDX41 in pre-rRNA processing, giving rise to a certain "ribosomal stress." In humans, the 18S, 5.8S, and 28S rRNA molecules are transcribed by RNA polymerase I as a single precursor called 47S pre-rRNA [23], which is then modified and cleaved post-transcriptionally into mature rRNA (Supplementary Figure E1B) [24]. The processing of pre-rRNA occurs mainly in the nucleolus, where ~4,500 putative nucleolar proteins and small nucleolar RNAs are thought to participate in this process [25]. Although the molecular functions of almost none of the nucleolar proteins have been elucidated (with some exceptions), a recent study

that performed siRNA-mediated depletion of 625 candidate nucleolar proteins helped to explain the pre-rRNA processing machinery [9]. Because it has been shown that some spliceosomal factors, such as hPrp43/DHX15 RNA helicase, also participate in pre-rRNA processing [26,27], DDX41 could play multiple roles. We think that this pathway can at least partly account for the development of AML with cytopenias harboring the DDX41 p.R525H mutation. Hematopoietic stem cells have a low level of protein synthesis compared with differentiating or growing progenitor cells [28]. Assuming that AML stem cells with the DDX41 p.R525H mutation are constitutively in a low-protein synthesis status due to ribosomal stress, the cells could be able to be maintained under this stress, but they cannot proliferate or differentiate, which would explain in part the pathophysiology of a slowly growing AML.

In summary, we propose a mechanism of growth defect in hematopoietic cells triggered by p.R525H DDX41 occurring in the following order: (1) the p.R525H mutant inhibits pre-rRNA processing; (2) compromised ribosomal biogenesis as a result of impaired rRNA synthesis causes a release of ribosomal proteins that bind to MDM2; and (3) MDM2-mediated RB degradation is suppressed, eventually activating the RB pathway and resulting in the inhibition of E2F activity. Although this study uncovered a pathogenic role of p.R525H DDX41 in the slow growth rate of tumor cells, how the mutation induces AML development and inhibits cell differentiation is still not understood. Lethally irradiated mice transplanted with hematopoietic stem/progenitor cells overexpressing p.R525H DDX41 did not develop myeloid malignancy, even in the p53-deficient background (Supplementary Figure E4B, online only, available at www.exphem.org). Considering the late occurrence of AML in patients harboring the mutation, age-dependent epigenetic alterations or other somatic changes may be required for this mutation to transform hematopoietic cells fully.

Acknowledgments

The authors thank Dr. H. Kawamoto for providing the cells and R. Tai, E. Kanai, and M. Nakamura for excellent technical assistance. This work was partly supported by the Daiichi Sankyo Foundation of Life Science, the NOVARTIS Foundation (Japan) for the Promotion of Science, the SGH Foundation, the Princess Takamatsu Cancer Research Fund, and the Relay for Life program founded by the Japan Cancer Society.

Conflict of interest disclosure

The authors declare no competing financial interests.

References

1. Polprasert C, Schulze I, Sekeres MA, et al. Inherited and somatic defects in DDX41 in myeloid neoplasms. Cancer Cell. 2015;27:658–670.
2. Lewinsohn M, Brown AL, Weinel LM, et al. Novel germ line DDX41 mutations define families with a lower age of MDS/AML onset and lymphoid malignancies. Blood. 2016;127:1017–1023.
3. Sekine R, Kitamura T, Tsuji T, Tojo A. Efficient retroviral transduction of human B-lymphoid and myeloid progenitors: Marked inhibition of their growth by the Pax5 transgene. Int J Hematol. 2008;87:351–362.
4. Ding L, Ley TJ, Larson DE, et al. Clonal evolution in relapsed acute myeloid leukemia revealed by whole-genome sequencing. Nature. 2012;481:506–510.
5. Parvatiyar K, Zhang Z, Teles RM, et al. The helicase DDX41 recognizes the bacterial secondary messengers cyclic di-GMP and cyclic di-AMP to activate a type I interferon immune response. Nat Immunol. 2012;13:1155–1161.
6. Zhang Z, Yuan B, Bao M, Lu N, Kim T, Liu YJ. The helicase DDX41 senses intracellular DNA mediated by the adaptor STING in dendritic cells. Nat Immunol. 2011;12:959–965.
7. Subramanian A, Tamayo P, Mootha VK, et al. Gene set enrichment analysis: A knowledge-based approach for interpreting genome-wide expression profiles. Proc Natl Acad Sci U S A. 2005;102:15545–15550.
8. Aspesi A, Pavesi E, Robotti E, et al. Dissecting the transcriptional phenotype of ribosomal protein deficiency: Implications for Diamond-Blackfan Anemia. Gene. 2014;545:282–289.
9. Tafforeau L, Zorbas C, Langhendries JL, et al. The complexity of human ribosome biogenesis revealed by systematic nucleolar screening of pre-rRNA processing factors. Mol Cell. 2013;51:539–551.
10. Linder P, Jankowsky E. From unwinding to clamping: The DEAD box RNA helicase family. Nat Rev Mol Cell Biol. 2011;12:505–516.
11. Dutt S, Narla A, Lin K, et al. Haploinsufficiency for ribosomal protein genes causes selective activation of p53 in human erythroid progenitor cells. Blood. 2011;117:2567–2576.
12. Ebert BL, Pretz J, Bosco J, et al. Identification of RPS14 as a 5q-syndrome gene by RNA interference screen. Nature. 2008;451:335–339.
13. Fumagalli S, Ivanenkov VV, Teng T, Thomas G. Suprainduction of p53 by disruption of 40S and 60S ribosome biogenesis leads to the activation of a novel G2/M checkpoint. Genes Dev. 2012;26:1028–1040.
14. Sun XX, Wang YG, Xirodimas DP, Dai MS. Perturbation of 60 S ribosomal biogenesis results in ribosomal protein L5- and L11-dependent p53 activation. J Biol Chem. 2010;285:25812–25821.
15. Durland-Busbice S, Reisman D. Lack of p53 expression in human myeloid leukemias is not due to mutations in transcriptional regulatory regions of the gene. Leukemia. 2002;16:2165–2167.
16. Sato S, Li K, Kameyama T, et al. The RNA sensor RIG-I dually functions as an innate sensor and direct antiviral factor for hepatitis B virus. Immunity. 2015;42:123–132.
17. Jiang F, Ramanathan A, Miller MT, et al. Structural basis of RNA recognition and activation by innate immune receptor RIG-I. Nature. 2011;479:423–427.
18. Fuller-Pace FV. DEAD box RNA helicase functions in cancer. RNA Biol. 2013;10:121–132.
19. Dardenne E, Pierredon S, Driouch K, et al. Splicing switch of an epigenetic regulator by RNA helicases promotes tumor-cell invasiveness. Nat Struct Mol Biol. 2012;19:1139–1146.
20. Abdul-Ghani M, Hartman KL, Ngsee JK. Abstrakt interacts with and regulates the expression of sorting nexin-2. J Cell Physiol. 2005;204:210–218.
21. Donati G, Brighenti E, Vici M, et al. Selective inhibition of rRNA transcription downregulates E2F-1: A new p53-independent mechanism linking cell growth to cell proliferation. J Cell Sci. 2011;124(Pt 17):3017–3028.
22. Uchida C, Miwa S, Kitagawa K, et al. Enhanced Mdm2 activity inhibits pRB function via ubiquitin-dependent degradation. EMBO J. 2005;24:160–169.

23. Baatout S. Staining of the nucleolar organizer regions: relevance in hematology. Blood Rev. 1996;10:185–188.
24. Mullineux ST, Lafontaine DL. Mapping the cleavage sites on mammalian pre-rRNAs: Where do we stand? Biochimie. 2012;94:1521–1532.
25. Ahmad Y, Boisvert FM, Gregor P, Cobley A, Lamond AI. NOPdb: Nucleolar Proteome Database—2008 update. Nucleic Acids Res. 2009;37(Database issue):D181–D184.
26. Bohnsack MT, Martin R, Granneman S, Ruprecht M, Schleiff E, Tollervey D. Prp43 bound at different sites on the pre-rRNA performs distinct functions in ribosome synthesis. Mol Cell. 2009; 36:583–592.
27. Yoshimoto R, Okawa K, Yoshida M, Ohno M, Kataoka N. Identification of a novel component C2ORF3 in the lariat-intron complex: Lack of C2ORF3 interferes with pre-mRNA splicing via intron turnover pathway. Genes Cells. 2014;19:78–87.
28. Buszczak M, Signer RA, Morrison SJ. Cellular differences in protein synthesis regulate tissue homeostasis. Cell. 2014;159: 242–251.

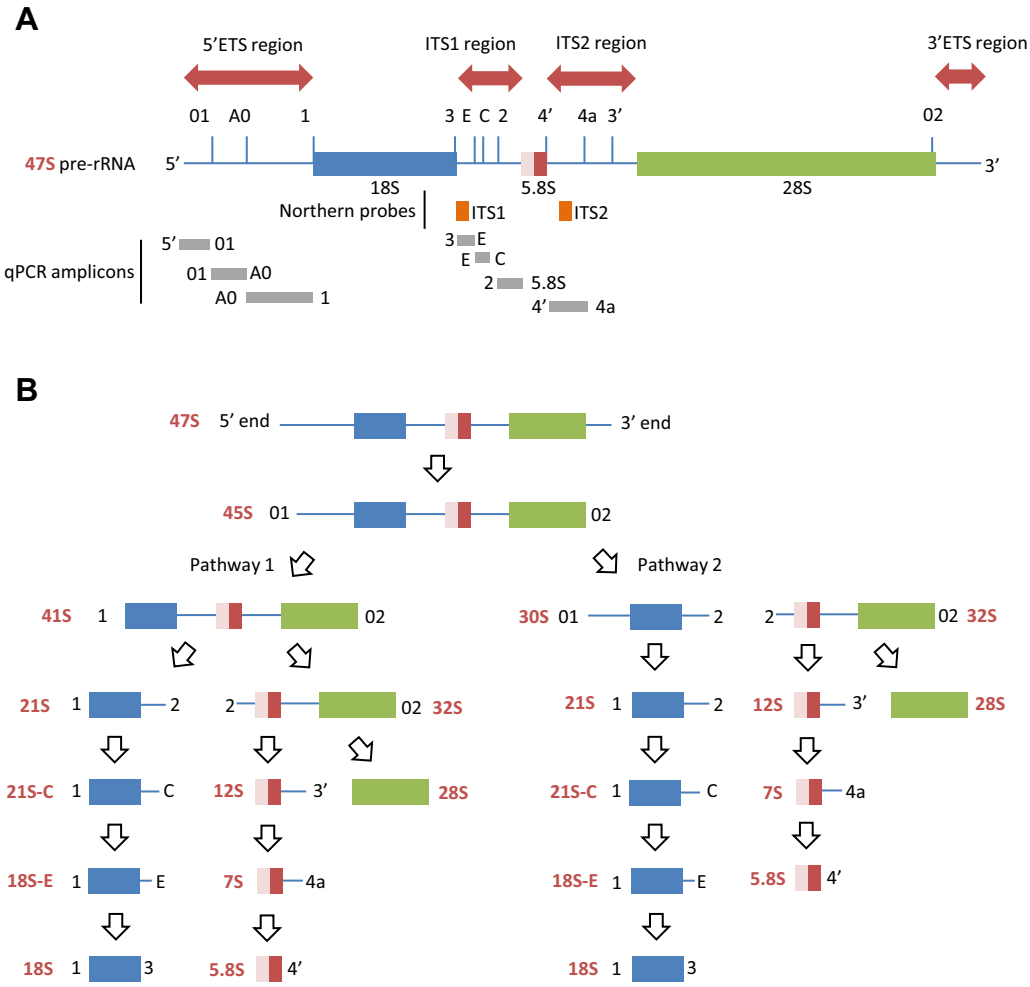

Supplementary Figure E1. Structure and processing pathways of pre-rRNA. (**A**) Structure of 47S pre-rRNA. The 5′ and 3′ ETS and ITS 1 and 2 are spacer regions that will be removed during pre-rRNA processing, and there are many pre-rRNA intermediates partially retaining these spacers, as shown in (**B**). Detailed pre-rRNA cleavage sites and their names are described in a recent review [24]. The regions used for northern probes (ITS1 and ITS2) and amplified by quantitative PCR analysis (5′-01, 01-A0, A0-1, 3-E, E-C, 2-5.8S, and 4′-4a) are shown in orange and gray, respectively. (**B**) Schematic processing pathways of pre-rRNA. Three rRNAs (18S, 5.8S, and 28S) are first transcribed as a long polycistronic precursor designated as 47S pre-rRNA. The latter will subsequently be processed to produce mature rRNAs through pathways, as shown in this schema.

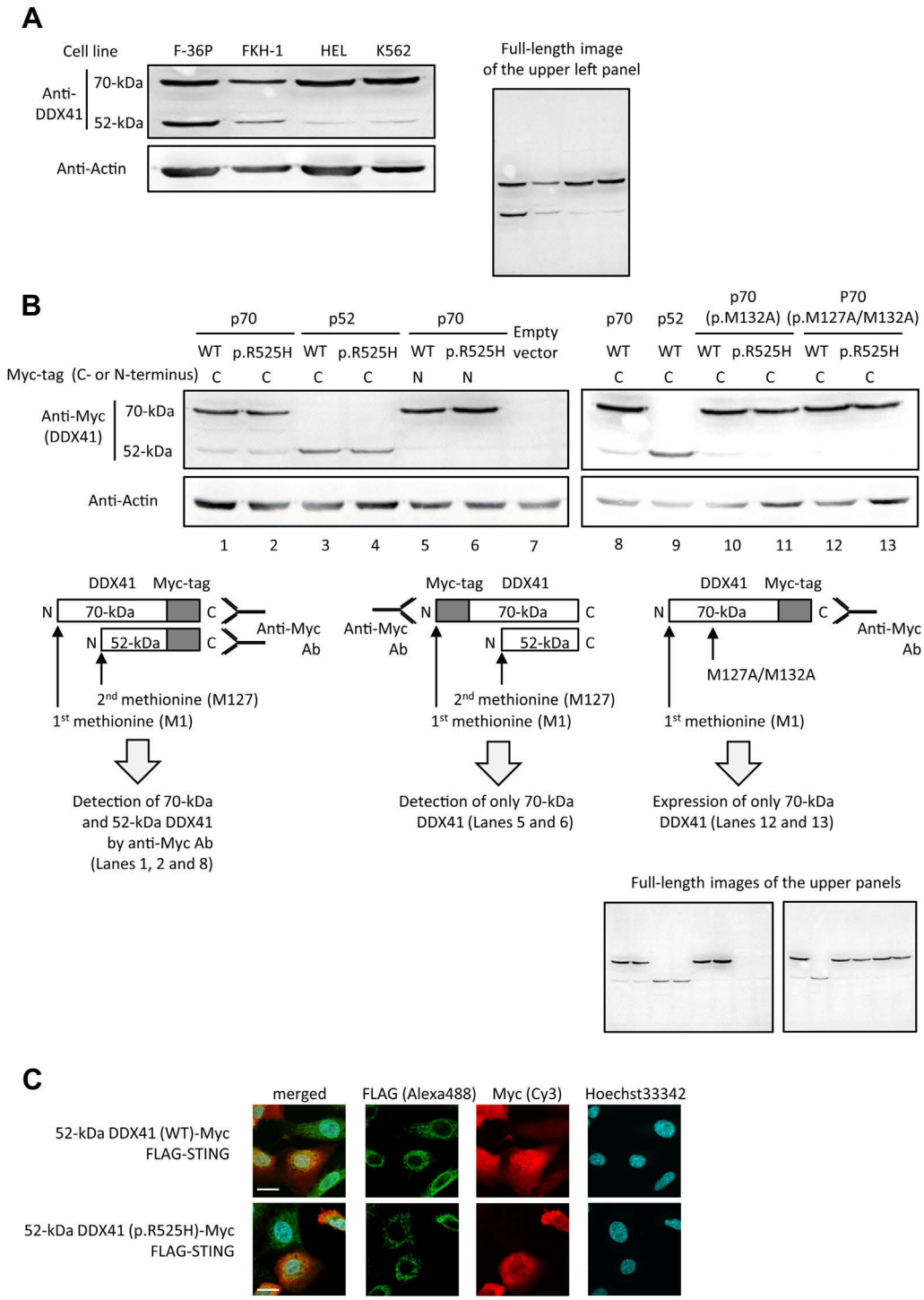

Supplementary Figure E2. Expression and localization of DDX41 and its short isoform. (**A**) Endogenous DDX41 expression in four AML cell lines (upper panels). DDX41 was detected by an antibody against the C-terminus of DDX41. A full-length image of DDX41 immunoblot is shown at right. (**B**) Exogenous DDX41 proteins expressed in HEK293 cells. The cells were transfected with a Myc-tagged DDX41 cDNA (cDNA starting from the first and second methionine, designated as p70 and p52, respectively), and the extracts were subjected to immunoblot analysis. Tagging positions are indicated as C (C-terminus) or N (N-terminus). The C-terminally tagged p70 cDNA also showed the 52-kDa band weakly (lanes 1 and 2), whereas the p70 cDNA tagged at the N-terminus did not show the 52-kDa band (lane 5 and 6), suggesting that the 52-kDa band is a truncated protein originated from the c-terminal part of DDX41. Indeed, the p70 cDNA, where the p.M132 (the third methionine) was substituted with an alanine, expressed a very weak 52-kDa band (lane 11), which disappeared when the p.M127 (the second methionine) was substituted with alanine (lanes 13 and 14). Actin was used as a loading control. A schematic diagram is shown in the center, and full-length images of DDX41 immunoblot are shown at bottom right. (**C**) Localization of 52-kDa DDX41 tagged with Myc at its c-terminus. The experiment was performed as in (**A**). Scale bars, 20 μm.

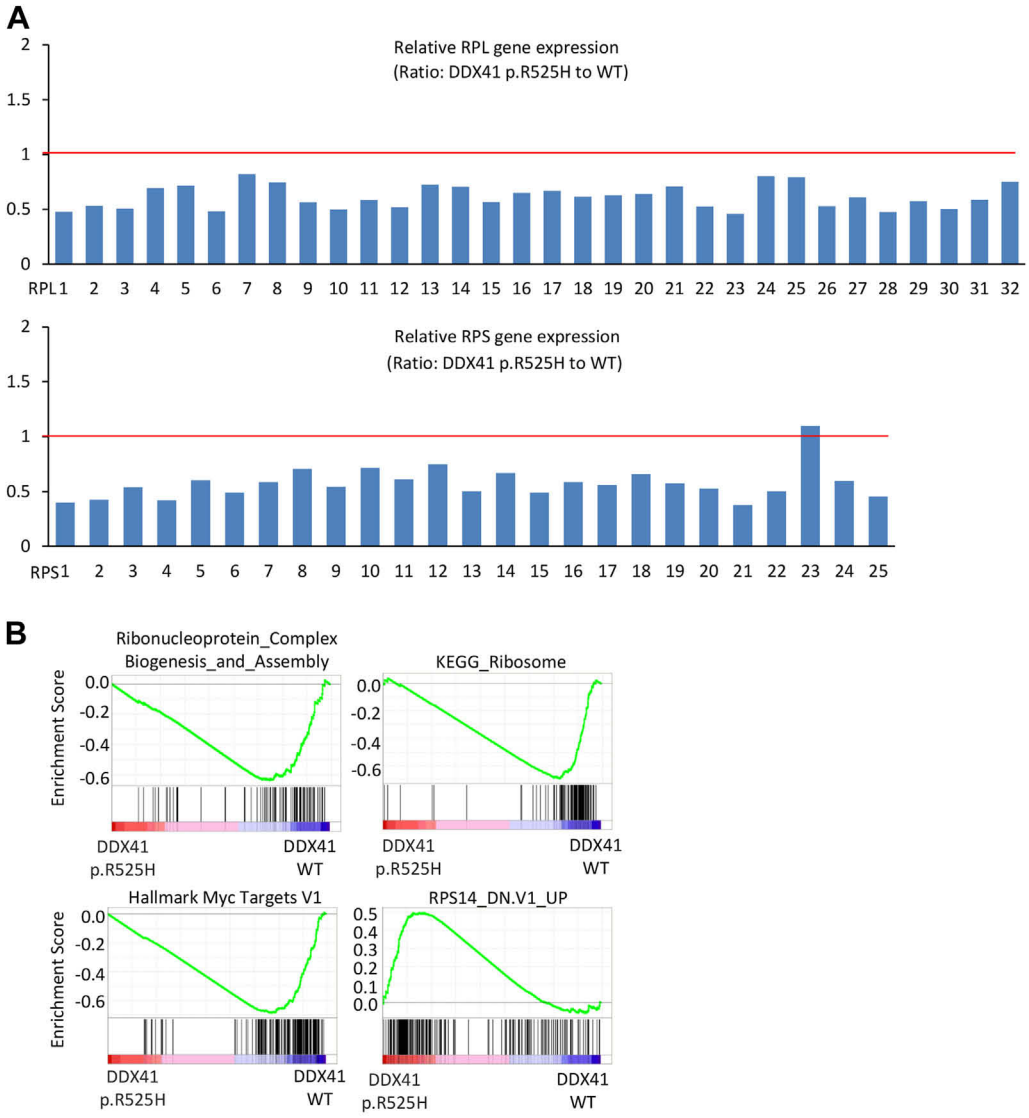

	Ribonucleoptotein Complex Biogenesis and Assembly	KEGG Ribosome	Hallmark Myc Targets V1	RPS14 DN.V1_UP
Normalized Enrichment Score	-1.94	-1.67	-2.28	1.73
Nominal p-value	0.0	0.003	0.0	0.0
FDR q-value	0.006	0.008	0.0	0.001

Supplementary Figure E3. Suppression of ribosomal genes in p.R525H DDX41-expressing cord blood cells. (**A**) Decrease in ribosomal genes (RPLs and RPSs) in p.R525H DDX41 cord blood cells compared with the cells transfected with WT DDX41-expressing vector. Each bar indicates the ratio of p.R525H cells to WT cells. (**B**) GSEA analysis indicating negative enrichment of gene sets related to ribosome biogenesis and positive enrichment of genes upregulated in RPS14-deficient p.R525H DDX41 cord blood cells. Normalized enrichment score, nominal *p* value, and FDR *q* value are shown at the bottom.

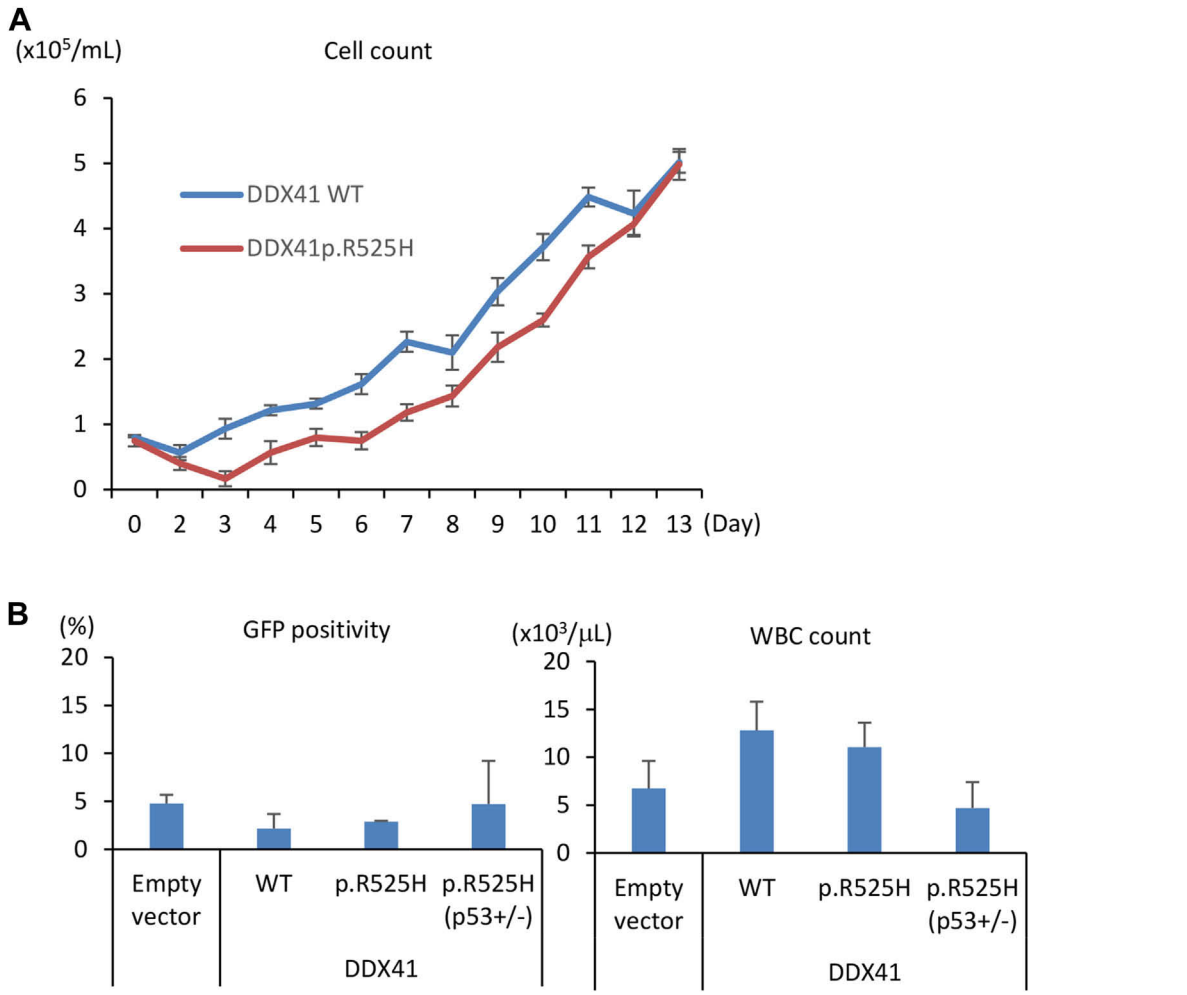

Supplementary Figure E4. There was no growth advantage of p.R525H DDX41-expressing cells in vitro or in vivo. (**A**) DDX41 (WT or p.R525H)-expressing THP-1 cell number. THP cells lacking functional p53 were transduced with a DDX41-expressing vector, and viable cells were counted. (**B**) There was no growth advantage of p.R525H DDX41-expressing hematopoietic cells in murine BMT experiments. Donor cells (with or without $p53^{+/-}$ background) were transduced with an empty/GFP-expressing vector or a DDX41/GFP-expressing vector, followed by transplantation into lethally irradiated recipients. GFP positivity (%) and peripheral WBC numbers ($\times 10^3/\mu L$) were measured 2–3 months after BMT. No significant difference in GFP signals was observed between the groups, suggesting that enforced expression of DDX41 pR525H alone does not account for the acquisition of clonogenicity.